Petroleum Research xxx (xxxx) xxx

Contents lists available at ScienceDirect

Petroleum Research

journal homepage: http://www.keaipublishing.com/en/journals/petroleum-research/

# Determination of total organic carbon content using Passey's method in coals of the central Kalahari Karoo Basin, Botswana

Mamphedi Sylvia Mabitje, Mimonitu Opuwari*

*Petroleum Geoscience Research Group, Department of Earth Sciences, University of the Western Cape, Cape Town, South Africa*

ARTICLE INFO

*Article history:*
Received 26 November 2021
Received in revised form
3 June 2022
Accepted 5 June 2022
Available online xxx

*Keywords:*
Passey's method
Vitrinite reflectance
Total organic carbon
Coal
Ultimate analysis
Central Kalahari Karoo basin

ABSTRACT

This paper focuses on determining total organic carbon (TOC) from boreholes in the Kalahari Basin, Botswana, using Passey's method. The Kalahari Karoo basin is one of several basins in southern Africa filled with Late Carboniferous to Jurassic sedimentary strata that host Permian age coal seams. Nine exploration boreholes (wells) drilled in the central Kalahari Karoo basin are used to determine the Total Organic Carbon potential. Vitrinite reflectance ($R_o$), proximate and ultimate analyses were conducted on cored coal intervals. Passey's ΔLogR method applied in this study employs resistivity and porosity logs to identify and quantify potential source rocks. Results of Passey's method compared with laboratory-measured carbon showed that Passey's method effectively identifies coal intervals. In terms of TOC calculations, the method works poorly in coal metamorphosed by dolerite intrusions. The heat affected coal samples had $R_o$ from 0.77% to 5.53% and increased in maturity from primarily maceral controlled to high volatile bituminous and anthracite coal. Results from proximate analysis showed compositional changes in the coal were controlled by proximity to sill intrusion, with a decrease in Fixed Carbon and an increase in ash yield in the contact metamorphism zone (2–12 m from sill). For the unaltered coal that has undergone burial maturation displaying $R_o$ of 0.44%–0.65%, the method works well. In unintruded boreholes, correlations between Carbon and calculated TOC indicate strong relationships. Passey's ΔLogR method proved to be a suitable method of estimating TOC on coal that has undergone burial maturation. This study has demonstrated that TOC calculated from the sonic log is more reliable in coal not affected by contact metamorphism than TOC calculated from the density log.


## 1. Introduction

Total Organic Carbon (TOC) content estimation is an essential component in source rock evaluation (Fertl and Chilingar, 1988; Kamali and Mirshady, 2004; Amiri Bakhtiar et al., 2011; Jarvie, 2012; Wang et al., 2016; Nyakilla et al., 2022). One of the indirect methods for the determination of TOC from well logs is from Passey's 1990 approach. The TOC content can also be used to determine fluid saturation and porosity in the formation evaluation because of the effects of organic matter on reservoir properties (Passey et al., 1990; Sondergeld et al., 2010; Alfred and Vernik, 2012; Li et al., 2014; Zhao et al., 2017).

Coal type refers to coals depositional origin and the maceral–mineral admixture resulting from that origin. Coal types typically fall into two categories: humic coals, developed from peat, and sapropelic coals, created from organic mud (O'Keefe et al., 2013). Shale in kerogen type is increasingly becoming an exploration target in many basins across the world as a potentially significant hydrocarbon generating source (Singh and Singh, 1994; Ogala, 2011; Singh, 2012; Zhang et al., 2018; Akanksha et al., 2020; Mohammed et al., 2019, 2020; Panwar et al., 2020). Kubu Energy acquired coal prospecting licences for three blocks (Fig. 1) within the Central Kalahari Karoo Basin, Botswana. Exploration in the basin revealed that methane concentrations in the coal seams of the Morupule and Serowe Formations' are under-saturated. Desorbed gas contents range between <1 and ≈ 2 $m^3$/t, with a few higher readings associated with dolerite intrusions (Faiz et al., 2013).

Coal bed methane (CBM) isalso known as coal seam gas (CSG), coal seam methane (CSM), and coal seam natural gas (CSNG). CBM forms as a thermogenically or biogenically derived gas (Moore, 2012)Methane occurs within the coal seam as adsorbed gas

* Corresponding author.
*E-mail address:* mopuwari@uwc.ac.za (M. Opuwari).

https://doi.org/10.1016/j.ptlrs.2022.06.002

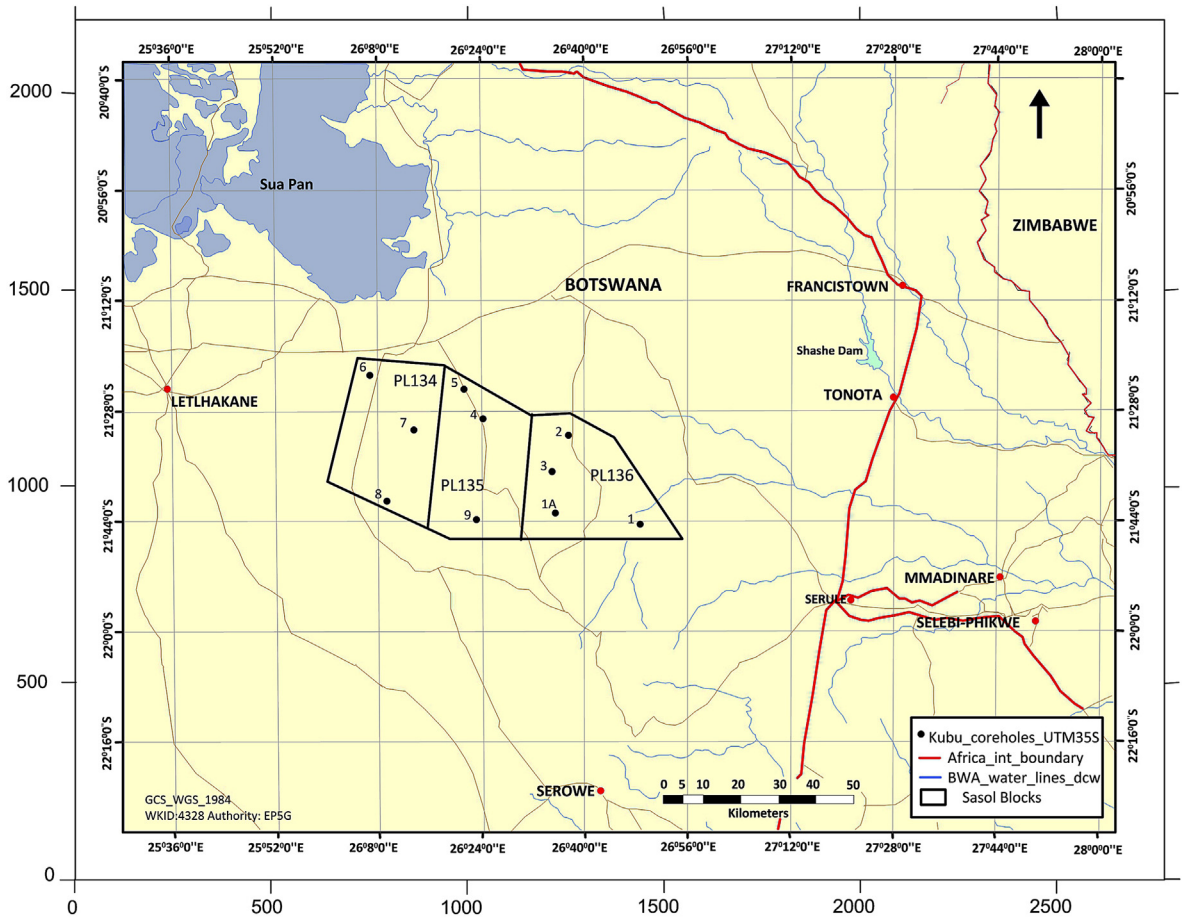


**Fig. 1.** Location of the nine exploration boreholes in central Botswana within Kudu licensed area (modified after Mabitje, 2016).

within the molecular structure of coal, and a small amount is stored as free gas in fractures and some in solution with water (Rao et al., 2014; Li et al., 2019; Singh et al., 2019; Tao et al., 2019). CBM may be accompanied by variable proportions of carbon dioxide and water, which are coal formation by-products (Singh, 2011; Rao et al., 2014; Zhu et al., 2019; Mendhe, 2020). The production of methane depends on the thickness, rank and maceral composition of the host coal. CBM occurs as biogenic (microbial) or thermogenic gas. Thermogenic gases have been associated with high rank coal, whereas microbial gases are produced at the early stages of the coalification process (Cokar et al., 2010; Rao et al., 2014; Song et al., 2018; Kalkreuth et al., 2020). The maceral composition of the Central Kalahari Karoo Basin's coal seams may have had a significant influence on the gas generation potential of the coal, dominated by vitrinite and inertinite groups with subsidiary quantities of liptinite; however, stratigraphically older coals contain less vitrinite and have higher inertinite contents (Bennett, 1989; Faiz et al., 2013; Bulguroglu and Milkov 2020).

The primary factor determining if a source rock can produce any hydrocarbons is thermal maturity (Shiri et al., 2013). Vitrinite reflectance ($R_o$) is the most commonly used maturation indicator of organic matter in sedimentary rocks. Vitrinite is a maceral group found in coals, in coaly inclusions in shales and disseminated in other sedimentary rocks. A method developed by Hood et al. (1975) for quantifying thermal maturity, which directly correlates to vitrinite reflectance, is the "level of organic metamorphism" (LOM). LOM is a scale that describes the degree of thermal metamorphism of organic matter with burial and it is used to measure the level of maturity of organic matter (Hood et al., 1975). Temperature controls the conversion of kerogen to hydrocarbon molecules. The level of organic matter metamorphism is attributed to geological time and palaeogeothermal gradients resulting from uplift and erosion (Hood et al., 1975; Price, 1983; Singh et al., 2016). The coal rank provides a basic framework for studying the process of coalification. This framework is used effectively in comparing LOM stages in petroleum generating source rocks. The numerical scale to estimate the level of maturity of organic matter developed by Hood et al. (1975) ranges from zero, indicative of no burial to twenty, at the point of anthracite/meta-anthracite boundary, and covers the entire range from the onset of petroleum generation to its overmaturity stage (Hood et al., 1975; Singh, 2011; Yu et al., 2017; Yelwa et al., 2021).

Wireline logs are an inexpensive and available method to extract information relating to the subsurface conditions and rock properties (Rider and Kennedy, 2002; Ramiah et al., 2019; Saffou et al., 2020; Opuwari et al., 2022). It is common practice to use, amongst other methods, Passey's ΔLogR technique to evaluate total organic carbon (TOC) using resistivity and porosity logs (Passey et al., 1990; Shiri et al., 2013). In industry, the application of Passey's ΔLogR technique has proven to be a practical approach for estimating TOC in source rocks (Kamali and Mirshady, 2004; Zhu et al., 2019; Liu et al., 2021).

Passey's method involves the overlaying of an adequately scaled porosity log on a deep resistivity curve. Sonic and density logs are commonly used as the porosity indicator logs (Rider and Kennedy, 2002; Rider, 2002; Opuwari, 2010; Opuwari, 2010, 2010; Magoba

and Opuwari, 2020; Magoba and Opuwari, 2020, 2020; Ayodele et al., 2021). Sonic and resistivity log readings in low resistivity shale are referred to as the baseline readings (Asquith and Gibson, 1982). These readings will vary with the depth of burial and geologic age. This technique assumes that the baseline condition will occur at the non-source interval (Passey et al., 1990; Charsky and Herron, 2013; Sun et al., 2013; Yu et al., 2017).

This study examines if Passey's method can identify coal bearing rocks of the Central Kalahari Karoo Basin as organic carbon-rich zones. This method will also be used to quantify the TOC in the coal-bearing formations. Passey's calculated TOC percentage will be compared to the ultimate analysis's carbon measurements to test this technique's validity.

## 2. Geological background

The Kalahari Karoo basin is one of several southern African basins filled with Late Carboniferous to Jurassic sediment that are primary targets for Permian coal (Bordy et al., 2010a; Franchi et al., 2021). The basin covers approximately 70% of Botswana, trending Northeast-Southwest (Johnson et al., 1996; Modie and Le Hérissé, 2009; Franchi et al., 2021). It is divided into five sub-basins based on geological setting and facies changes (Smith, 1984). The Central Kalahari Karoo Basin is further sub-divided into southern, northern, western and south East Central Kalahari belts for descriptive purposes (Smith, 1984). This study's focus area is within the eastern part of Botswana (Fig. 1) in the Northern and South East Central Kalahari belts, within three production licenses (PL134, PL135 and PL136) in 2012–2013 (Faiz et al., 2013; Bulguroglu and Milkov 2020).

The Kalahari Karoo Basin and its subsidiary basins remain little understood in terms of their exact geodynamic setting. Some studies (Visser, 1997; Catuneanu et al., 2005; Haddon, 2005) have attributed these sub-basins to collision-induced extensional tectonics, related to the Late Palaeozoic to Early Mesozoic Gondwanide-Cape orogeny that resulted from the subduction of a palaeo-Pacific plate under southern Gondwana. This led to the Karoo Basin's development in the south as a retro-arc foreland basin to the Cape Fold Belt.

The Kalahari Karoo Basin's sub-surface structural framework is little understood due to the Kalahari Group sediments' extensive nature, generally 60–100 m thick and reaches 400 m thickness in the central Kalahari. Fault-bounded graben structures have been identified along the basin's eastern margin, exposed on the surface. The dyke swarm in central Botswana represents one of the significant fissure of intrusive complexes in the world (Le Gall et al., 2002). This complex forms a 1500 km long and 100 km wide tectono-magmatic structure extending from western Zimbabwe through Botswana and northern Namibia. The strike complex trends at 110° east. The individual dyke intrusions dip between 60 and 90° to the north-east. These dyke intrusions cut through Archaean basement terranes and Permo- Jurassic sedimentary sequences (Le Gall et al., 2002).

The stratigraphy of the Kalahari Karoo Basin records a transition from a glacial period to fluvio-deltaic and swampy periods and ultimately turns arid before the extrusion of continental flood basalts (Smith, 1984; Visser, 1997). The Kalahari Karoo Basin's stratigraphic nomenclature is adopted mainly from the South African Karoo stratigraphy it is well exposed (Smith, 1984; Catuneanu et al., 2005; Bordy et al., 2010b).

## 3. Materials and methods

This study's data includes wireline logs, proximate analysis results, and vitrinite reflectance measurements for exploration boreholes CH1 to CH9. Vitrinite reflectance measurements were not conducted on all cored intervals, only four to five samples were selected per borehole. Vitrinite reflectance was used to determine thermal maturity on coal samples as this is an essential parameter in the TOC calculations.

Andersen Geological Consulting of South Africa conducted the geophysical logging of exploration boreholes (CH1–CH9). Wireline logs were provided for all nine boreholes, and they included gamma-ray (GR), density, resistivity and sonic logs.

The histogram distributions of log measurements were used to set a limit or baseline for different rock type classification. For example, a histogram distribution of GR logs for all boreholes, used to classify lithology types based on clay content, is presented in Fig. 2. The mean GR value, which is 113.27 API, was used as a cut off value for differentiation. Below 113.27 °API, lithology was identified as dolerite, coal or sandstone or siltyclaystone. Above 113.27 °API, the lithology was considered as claystone. The density log distribution histogram served to segregate intervals with gamma-ray values less than 113.27° API into either dolerite, coal or silty mudstone. Table 1 shows log measurement ranges used to characterise lithology types (Amini et al., 2014; Mabitje, 2016; Opuwari et al., 2021; Opuwari and Dominick, 2021).

### 3.1. Proximate and ultimate analysis

Proximate analysis AS 1038.3 (Standards Association of Australia, 2000a) was conducted. The proximate analysis involves determining the volatile matter, moisture, fixed carbon and ash yield (Warne, 1991). The procedure involves drying a known mass of coal in an oxygen-free (nitrogen flush) oven at 105–110 °C for a period of 1.5–3 h (Mayoral et al., 2001). After removing the sample from the oven and placing it in a desiccator, the coal was weighed, and the loss of mass ascribed to inherent moisture measured. The sample is then heated in a cylindrical silica crucible in a muffle furnace at 950 °C for 7 min to effect the removal of all volatile matter. During this process, the loss of mass recorded is equal to the

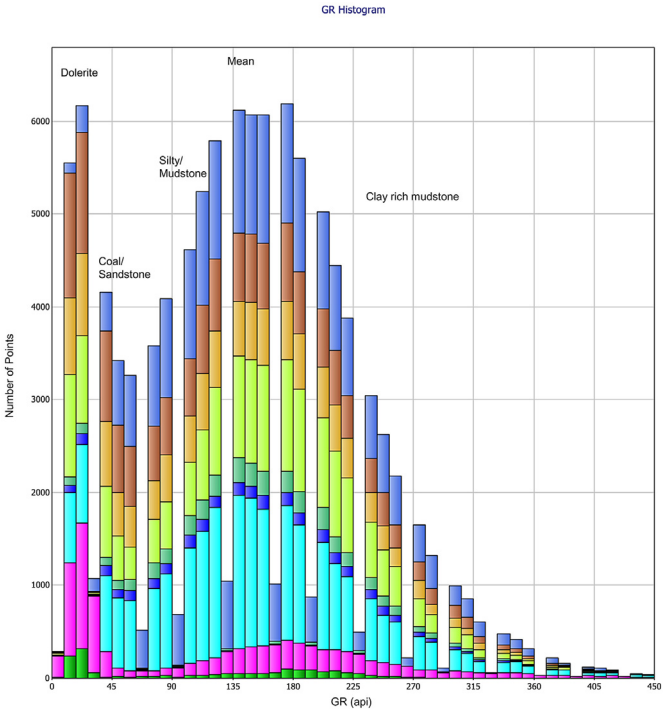


**Fig. 2.** Histogram distribution of clay content in all boreholes using gamma-ray curves.

**Table 1**
Approximate log measurement ranges used to characterise lithology types (modified after Mabitje (2016) and Sahoo et al. (2021)).

| Lithology | Gamma-ray (°API) | Density (g/cc) | Resistivity (ohm-m) | Sonic (μsec/m) |
|---|---|---|---|---|
| **Dolerite** | 3–21 | 2.7–3.2 | 110–1000 | 50–180 |
| **Coal** | 6–65 | 1.12–2.25 | 18–110 | 280–480 |
| **Silty Clastic** | 65–113 | 2.25–2.7 | 0.1–5 | 180–250 |
| **Clay rich** | 113–336 | 2.3–2.5 | 5–20 | 250–320 |

proportion of volatile matter present in the sample. Determination of ash yield is achieved by combusting the coal until a constant mass is attained by heating the sample to 500 °C for 30 min before increasing the temperature to 815 °C until combustion is complete. The ash percentage is calculated from the mass of the residue remaining after incineration. The amount of fixed carbon was not determined by direct measurement but calculated from the difference between the sums of all other components (Elder, 1983).

The ultimate analysis provides information on the elemental composition of coal, which are the proportions of carbon, hydrogen, nitrogen, oxygen, and sulphur for classification and application. For this analysis, a coal sample is combusted in an ultimate analyser, which measures the weight percentage of carbon, hydrogen, nitrogen, sulphur, and ash from a coal sample. The total carbon, hydrogen, and nitrogen are determined simultaneously from the same sample in the analyser. Total oxygen is calculated from the other values. The variations in chemical composition from the ultimate analysis data reflect variations in coal type and coal rank. The protocols from the testing method described by the Australian Standard for coal and coke analysis and testing method AS 2456.3 (Standard Association of Australia, 2000b) for ultimate analysis is used in this study.

### 3.2. Thermal maturity: vitrinite reflectance

Weatherford Laboratories conducted the vitrinite reflectance measurements according to the Australian Standards AS2456.3 (Standards Association of Australia, 2000b). A minimum of fifty readings were measured for each sample. Also, thermally affected samples displayed erreneous values and were noted in the report. Vitrinite reflectance measurements were then used to classify samples as immature, mature or post-mature, according to the ranking of Diesel (1992) and Teichmüller (1989) presented in Table 2.

Passey's ΔLogR method requires LOM value to convert the ΔLogR separation to a quantitative TOC. To determine LOM values from $R_o$ measurements, the $R_o$ values were supperimposed and correlated with Hood et al. (1975) coal rank numerical scale (Fig. 3) and equivalent LOM value obtained. The coal rank scale is from zero at burial to twenty, and it is subdivided within the sub-bituminous and high volatile bituminous coal rank classification. The estimated LOM with respect to vitrinite reflectance of the samples is presented in Table 3. The vitrinite reflectance was plotted as a function of LOM (Fig. 4), and a relationship for the estimation of LOM from $R_o$ was established as follow:

$$LOM = 0.004\ (R_o^3) - 0.4987\ (R_o^2) + 5.1115\ (R_o) + 5.5714 \quad (1)$$

Using the relationship between LOM and $R_o$ established in Fig. 4, Table 3 was created to assign $R_o$ measurements their corresponding LOM values. Based on the established correlation, a LOM value less than 8.46 correlates to thermally immature coal, and LOM values ranging from 8.46 to 10.59, 10.59–11.76, and greater than 11.76 correspond to the oil window, the wet gas/condensate window, and the dry gas window, respectively.

### 3.3. Passey's method and input parameters

Passey's method for the determination of TOC uses the density, sonic, and deep resistivity curves. The density and sonic curves are individually overlain with the deep resistivity curve in an organic lean interval, and the overlap is defined as the baseline (Yu et al., 2017). A baseline exists when there is an overlap between two curves, resistivity/density and resistivity/sonic, or when the curves are close to each other in a relatively thick interval. An organic-rich source rock interval is recognised by a separation of the two curves (Fig. 5). The separation between the density/resistivity and sonic/resistivity is designated as Δlog R, which is related to TOC, and it can be measured at different depth intervals (Passey et al., 1990).

The baseline interval readings of 10 Ω m, 2.5 g/cc, and 300 μs/m were recorded for resistivity, density, and sonic logs, respectively. The sonic, density and resistivity logs were used to achieve DlogR (density resistivity) and SlogR (sonic resistivity) separations. These separations were quantified and then used together with individual

**Table 2**
Phases of petroleum generation with their corresponding vitrinite reflectance indices (Diesel, 1992; Teichmüller, 1989).

| Coal Rank | Ro (%) | LOM | Maturity Phase |
|---|---|---|---|
| Peat | <0.23 | <6.72 | Immature |
| Lignite | 0.23–0.36 | 6.72–7.35 | Immature |
| Sub-bituminous: C | 0.36–0.41 | 7.35–7.58 | Immature |
| Sub-bituminous: B | 0.41–0.47 | 7.58–7.86 | Immature |
| Sub-bituminous: A | 0.47–0.49 | 7.86–7.96 | Immature |
| High-Volatile Bituminous: C | 0.49–0.51 | 7.96–8.05 | Immature |
| High-Volatile Bituminous: B | 0.51–0.69 | 8.05–8.86 | Immature to Mature |
| High-Volatile Bituminous: A | 0.69–1.11 | 8.86–10.64 | Mature (Oil) |
| Medium-Volatile Bituminous | 1.11–1.6 | 10.64–12.49 | Mature(wet gas) |
| Low-Volatile Bituminous | 1.6–2.04 | 12.49–13.96 | Mature (dry gas) |
| Semi-Anthracite | 2.04–2.4 | 13.96–15.02 | Mature |
| Anthracite | 2.4–5 | 15.02–19.16 | Mature to Post Mature |
| Meta-Anthracite | >5 | >19.16 | Post Mature |

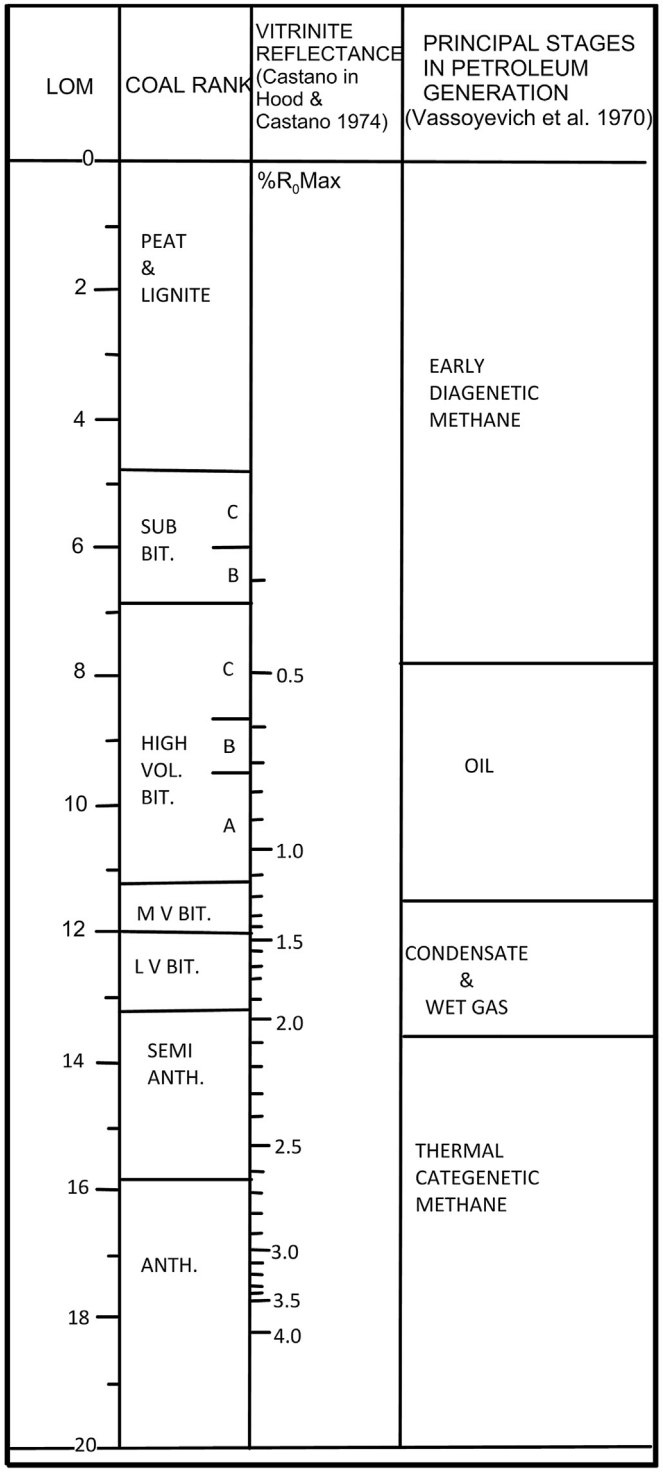


**Fig. 3.** Numerical scale relating coal rank, vitrinite reflectance ($R_o$) and petroleum generation stage to level of organic metamorphism (LOM) (modified after Hood et al., 1975).

LOM values as inputs in the TOCd (TOC calculated from density log) and TOCs (TOC calculated from the sonic log) calculations in Microsoft Excel. For the generation of TOC curves in IP Software, the same inputs were used, but instead of inserting raw data averages from spreadsheet listings in the equation, actual resistivity, density and sonic curves were used.

## 4. Results and discussion

### 4.1. Thermal maturity

The $R_o$ for all samples analysed indicate a wide range of measurements, from 0.4 to 5.53 (Fig. 6a). The geothermal gradient in the basin is approximately 36 °C/km (Haddon, 2005). The $R_o$ in CH1 and CH6 are between 0.44 and 0.65, indicating that coal in both boreholes is low to medium rank. Also, $R_o$ increases with depth (Fig. 6) in these boreholes, signifying the role played by diagenesis. These boreholes can be used for control and comparison of % Ro in boreholes affected by intrusions.

In boreholes CH2, CH3, CH4, CH5, CH7, CH8 and CH9, some coal intervals are affected by the heating from dolerite intrusions. The heating from dolerite intrusions is evident in their % Ro measurements ranging between 0.77% and 5.53% (Fig. 6). Intrusion on coal has been proven to increase the vitrinite reflectance values (Bostick and Pawlewicz, 1984; Stewart et al., 2005; Fjeldskaar et al., 2008). Coals in closest contact with intrusions show $R_o$> 5%, which rapidly decreases to 0.77% with increasing distance from the intrusion. This rapid decrease in $R_o$ suggests that intrusive events' contact metamorphism was probably confined to a few meters on either side of intrusion. The alteration of coal is highest at the contact and extends into the coal as an aureole (Golab, 2003; Jiang et al., 2011). The aureole size depends on the chemistry, temperature, degree of intrusion crystallisation, and volatile fluids (Golab, 2003).

Bennett (1989) found that coals of the Mamabula area in the Central Kalahari Karoo Basin have a mean maximum $R_o$ between 0.52 and 0.64. He attributed the immaturity of the coals to the basin dynamics and burial depths. The $R_o$ measurements of his study are consistent with CH1 and CH6, measured between 0.44 and 0.65. The borehole's $R_o$ values indicate that coals in the basin are primarily sub-bituminous type B to high volatile bituminous type B in rank. High volatile bituminous to anthracitic coals formed by rapid heating that occurred in localised areas adjacent to intrusions. In Table 3, samples at depth 374.10 m and 410.25 m of borehole CH3 are not thermally metamorphosed, whereas intervals above and below them are heat affected. Heat effects depend on the extent of the contact aureole for each sill.

Based on $R_o$ measurements and distance between coal intervals and sill in each borehole, the sill intrusion area is divided into three zones: (1) contact metamorphism zone, which is within 2–12 m from the sill, (2) thermal evolution zone, that is within distances of 12–54 m from the sill and (3) unaltered zone. The contact metamorphism zone displays $R_o$ from 3.67% up to 5.53; the thermal evolution zone has $R_o$ between 0.77% and 1.91. The unaltered zone is characterised by $R_o$ of between 0.44% and 0.65.

The heat affected samples are mostly mature, covering the oil, wet gas and condensate and dry gas windows. Their LOM ranges from 9.21 to 19.26, with post-mature samples yielding values more significant than 18.29. Heat effects accelerated the LOM of these coals. Non-heat affected samples from all boreholes show LOM values ranging from 7.72 to 8.68, and these are considered immature (Table 3). Corresponding LOM values in terms of the three zones of the intrusion area are 7.72–8.68, 9.21–13.54 and >17.81 for the unaltered, thermal evolution and contact metamorphism zones, respectively (Fig. 6b).

Similarly, with $R_o$, boreholes CH1 and CH6 display increasing LOM and rank with depth. In intruded boreholes CH2 and CH8 (Table 3), there is an increase of LOM with depth, probably because sill intrusions in both boreholes only occur adjacent to deeper sampled intervals. Therefore, an alteration was only experienced in these intervals governed by aureole dynamics where the coals in contact or adjacent to the intrusion will be heated the most. The intrusions have altered the relationship between maturity and

**Table 3**
A quantitative relationship between coal rank, $R_o$, LOM and indication of coal rank and maturity phases.

| Borehole | Depth | Coal Rank | VRo | LOM | Maturity Phase |
|---|---|---|---|---|---|
| | m | | % | | |
| CH1 | 246.12 | Sub- bituminous: B | 0.44 | 7.72 | Immature |
| CH1 | 268.80 | Sub- bituminous: B | 0.47 | 7.86 | Immature |
| CH1 | 275.50 | Sub- bituminous: A | 0.49 | 7.96 | Immature |
| CH1 | 277.76 | Sub- bituminous: B | 0.47 | 7.86 | Immature |
| CH1 | 279.9 | High-Volatile bituminous C | 0.5 | 8.00 | Immature |
| CH2 | 257.64 | Sub- bituminous: B | 0.46 | 7.82 | Immature |
| CH2 | 272.49 | High-Volatile Bituminous:A | 0.77 | 9.21 | Mature |
| CH2 | 276.51 | Medium Volatile Bituminous | 1.52 | 12.20 | Mature |
| CH2 | 297.20 | DOLERITE | | | |
| CH2 | 357.97 | Medium Volatile Bituminous | 1.57 | 12.38 | Mature |
| CH3 | 364.37 | High-Volatile Bituminous:A | 0.83 | 9.47 | Mature |
| CH3 | 374.10 | High-Volatile Bituminous:B | 0.52 | 8.10 | Immature |
| CH3 | 410.25 | High-Volatile Bituminous:B | 0.64 | 8.64 | Mature |
| CH3 | 418.44 | High-Volatile Bituminous:A | 0.92 | 9.85 | Mature |
| CH3 | 421.46 | Medium Volatile Bituminous | 1.39 | 11.72 | Mature |
| CH3 | 431.70 | DOLERITE | | | |
| CH4 | 381.00 | Low Volatile Bituminous | 1.91 | 13.54 | Mature |
| CH4 | 392.00 | DOLERITE | | | |
| CH4 | 438.25 | Meta Anthracite | 5.53 | 19.26 | Post Mature |
| CH4 | 451.19 | High-Volatile Bituminous:A | 0.84 | 9.52 | Mature |
| CH4 | 479.97 | High-Volatile Bituminous:A | 0.87 | 9.64 | Mature |
| CH4 | 488.31 | Medium Volatile Bituminous | 1.59 | 12.45 | Mature |
| CH6 | 319.78 | Sub- bitumonous: B | 0.45 | 7.86 | Immature |
| CH6 | 329.01 | High-Volatile Bituminous:C | 0.51 | 8.05 | Immature |
| CH6 | 420.22 | High-Volatile Bituminous:B | 0.60 | 8.46 | Mature |
| CH6 | 356.27 | High-Volatile Bituminous:B | 0.65 | 8.68 | Mature |
| CH7 | 404.28 | High-Volatile Bituminous:C | 0.50 | 8.00 | Immature |
| CH7 | 432.92 | High-Volatile Bituminous:B | 0.54 | 8.19 | Immature |
| CH7 | 440.22 | High-Volatile Bituminous:B | 0.54 | 8.19 | Immature |
| CH7 | 462.81 | High-Volatile Bituminous:B | 0.55 | 8.23 | Immature |
| CH7 | 485.62 | Anthracite | 3.88 | 18.13 | Mature |
| CH7 | 500.40 | DOLERITE | | | |
| CH8 | 374.29 | Sub-Bituminous −C | 0.40 | 7.54 | Immature |
| CH8 | 386.81 | High-Volatile Bituminous:B | 0.62 | 8.55 | Mature |
| CH8 | 391.07 | High-Volatile Bituminous:A | 0.90 | 9.77 | Mature |
| CH8 | 419.00 | DOLERITE | | | |
| CH9 | 406.40 | High-Volatile Bituminous:C | 0.51 | 8.05 | Immature |
| CH9 | 419.60 | DOLERITE | | | |
| CH9 | 421.30 | Anthracite | 3.67 | 17.81 | Mature |
| CH9 | 444.60 | Medium Volatile Bituminous | 1.30 | 11.38 | Mature |
| CH9 | 455.90 | DOLERITE | | | |
| CH9 | 504.60 | Anthracite | 4.71 | 19.00 | Post Mature |
| CH9 | 520.86 | Low Volatile Bituminous | 1.88 | 13.44 | Mature |
| CH9 | 525.90 | DOLERITE | | | |

depth in boreholes CH3, CH4, CH5 and CH9.

### 4.2. Proximate and ultimate analysis

The proximate analysis performed to determine the ash yield, moisture, volatile matter, and fixed carbon at the air-dry base and dry ash-free basis are presented in Table 4. The results indicate three clusters (Fig. 7) in the sample distribution. Cluster 1(green colour) is non-heat affected with $R_o$ ranging from 0.44% to 0.65. Cluster 2 (blue colour) samples are slightly heated to heat-affected with $R_o$ ranging between 0.77% and 1.91. Cluster 3 (red colour) is the devolatilized or coked coal samples with $R_o$ and greater. These clusters correspond to the three zones distinguished earlier. Cluster 1 displays the highest moisture content range from 2.42% to 6.36%, in cluster 2, the range is from 0.76% to 3.14%, and cluster 3 ranging from 1.3% to 3.4%. Surprisingly, the moisture of the slightly heat-affected samples is less than that of the devolatilized samples. According to Jiang et al. (2011), this may occur due to the intrusion acting as a seal to prevent moisture loss after the magmatic intrusion. This observation may hold as the devolatilized samples are within the contact metamorphism zone (2–12 m from nearest sill).

Cluster 3 displays the lowest volatile matter content proving that with increasing heat effects from intrusion, devolatilisation occurs. Thermally evolved cluster 2 shows higher fixed Carbon than cluster 1. These results are generally in agreement with those of Jiang et al. (2011) and (Rimmer et al., 2009), who both state that intrusions on coal seams result in increases in fixed Carbon and % Ro and decreases volatile matter and moisture adjacent to the igneous intrusion. Cluster 3 exhibits a decrease in fixed Carbon and an increase in ash yield with increasing $R_o$. According to Golab (2003), this is because, at higher temperatures where coking begins, vitrinite becomes porous, changes from anisotropic to isotropic and crystallises to form semi-coke.The liptinites spontaneously decompose, reflectance increases and all or part of the organic matter is removed by reactions that form carbon dioxide, methane and other products.

An exception in cluster 3, sample at depth 486.2 m of borehole CH7, interpreted as an anthracite coal rank with $R_o$ of 3.88 (Tables 3 and 4), displays the highest fixed carbon measurement of 67.18% and 22.10% ash content at air-dry basis, this is possible because it has not reached the post maturity phase of $R_o > 4$ and is in an early stage of semi-coking.

The ultimate analysis results found that the carbon percentage

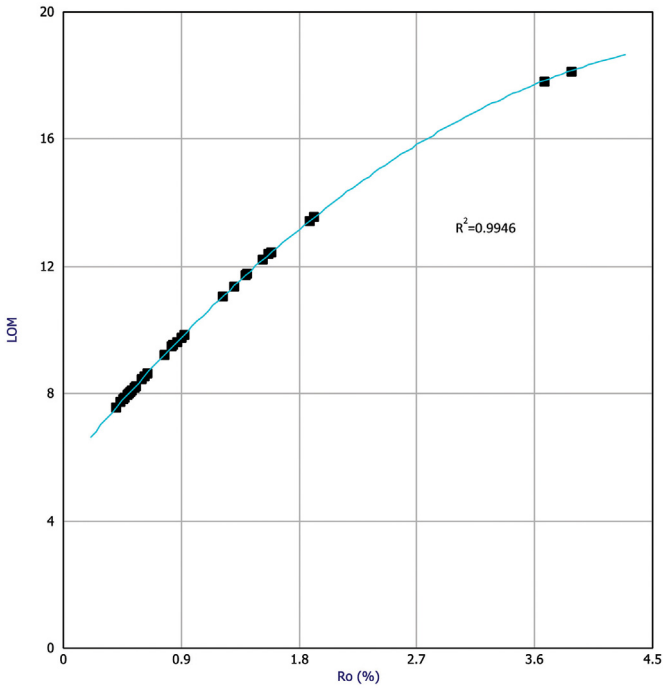


**Fig. 4.** Graphical representation of the relationship between $R_o$ and LOM.

varies from 71.1% to 91.0% (Table 5). The sulphur content is high, and the percentage varies from 0.55% to 10.55%. The calculated atomic H/C and O/C ratio for the samples ranged from 0.01 to 0.08 and 0.05 to 0.31, respectively. This result indicates that the samples are richer in humic coal than perhydrous coal, predominantly of sub-bituminous to bituminous coal (Diesel, 1992; Banik 2020; Takahashi et al., 2020).

It can be inferred from coal rank result (Table 3), proximate analysis (Table 4), and ultimate analysis results (Table 5) that there is a general trend of increase in vitrinite values with depth of caol except for borehole CH1.This observed trend was also reported by other researchers (Trent et al., 1982; Langenberg et al., 1992; Ward et al., 2005). Additionally, the vitrinite reflectance values increases with increase in fixed carbon (daf) and decrease in volatile matter content. There is an increase in carbon content with depth in borehole CH7 and CH8 (Table 5).

In comparison, the fixed carbon calculated from the proximate analysis (Table 4) is a different value (lower) than the total carbon value (higher) from the ultimate analysis (Table 5). The reason for the differences in values is attributed to the fact that the carbon from the ultimate analysis includes some organic carbon that escapes as volatile gaseous matter during combustion (Yi et al., 2017). The carbon percentages from the ultimate analysis are used to compare with log calculated TOC.

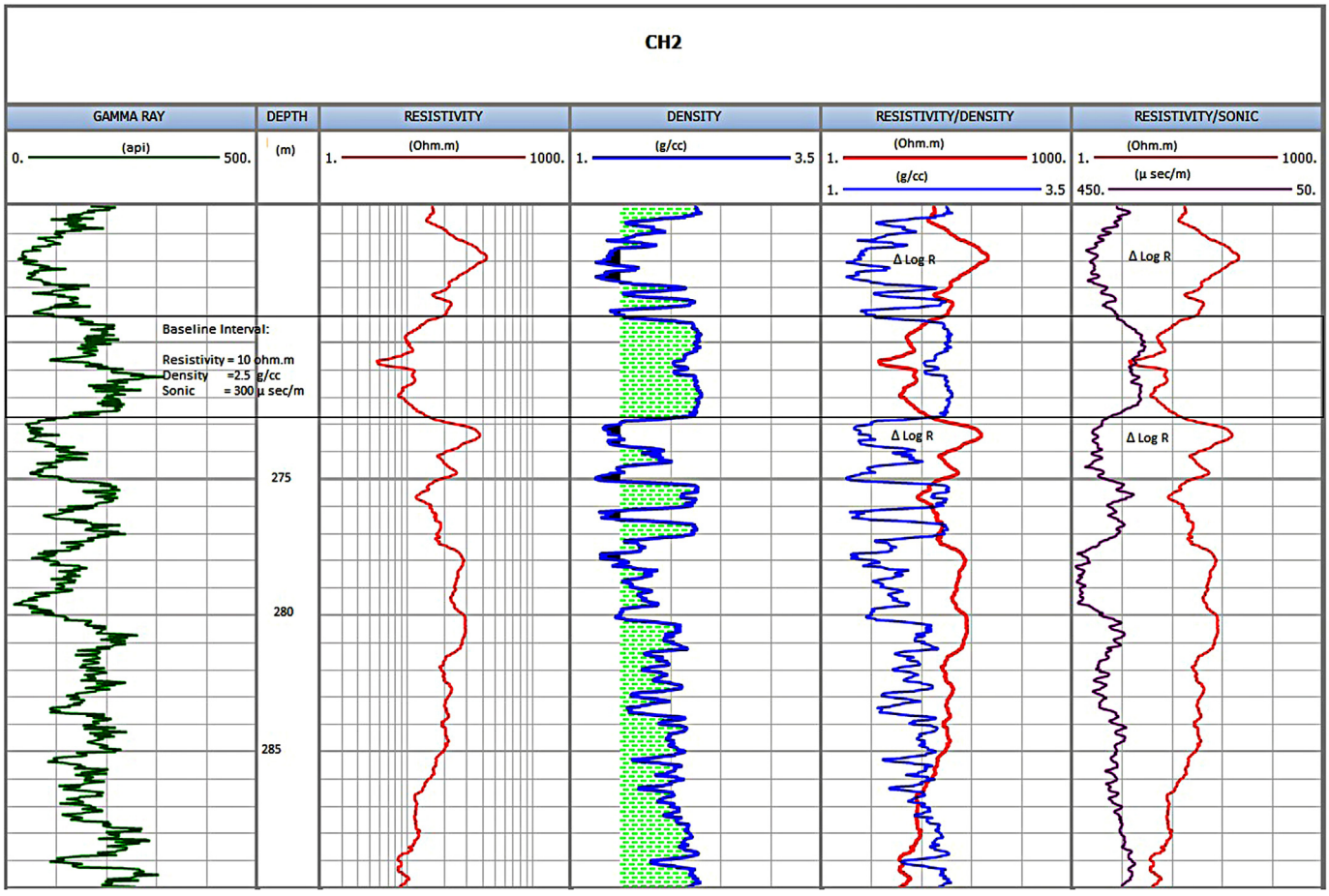


**Fig. 5.** Example of logs used to establish a baseline. The separation of the two curves recognises an organic-rich source rock interval. Gamma-ray log plotted in track 1, while the overlay of resistivity and density log is displayed in track 5, and overlay of resistivity and sonic logs are displayed in track 6.

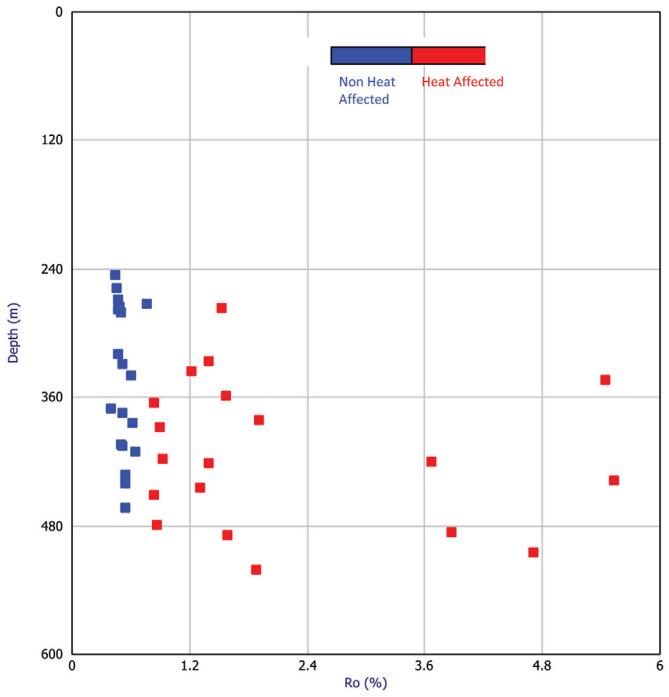


**Fig. 6.** Vitrinite reflectance ($R_o$) distribution with depth for all boreholes. $R_o$ trends with depth for coals heat-affected by dolerite intrusions and non-heat affected coals.

**Table 4**
Proximate analysis results of boreholes.

| Borehole | Depth | M | A | VM | FC | M | VM | FC |
|---|---|---|---|---|---|---|---|---|
| | m | % ad | % ad | % ad | % ad | % daf | % daf | % daf |
| CH1 | 245.82 | 5.65 | 22.11 | 28.74 | 43.49 | 7.25 | 36.90 | 55.84 |
| CH1 | 268.38 | 5.45 | 20.23 | 31.50 | 42.82 | 6.83 | 39.49 | 53.68 |
| CH1 | 275.24 | 5.43 | 21.04 | 30.70 | 42.84 | 6.88 | 38.88 | 54.26 |
| CH1 | 277.30 | 4.71 | 29.99 | 25.84 | 39.46 | 6.73 | 36.91 | 56.36 |
| CH1 | 279.96 | 5.08 | 12.37 | 32.94 | 49.62 | 5.80 | 37.59 | 56.62 |
| CH2 | 257.64 | 4.88 | 26.79 | 33.52 | 34.82 | 6.67 | 45.79 | 47.56 |
| CH2 | 272.49 | 2.69 | 26.84 | 27.69 | 42.78 | 3.68 | 37.85 | 58.47 |
| CH2 | 276.51 | 1.45 | 21.45 | 16.30 | 60.81 | 1.85 | 20.75 | 77.42 |
| CH2 | 297.20 | | DOLERITE | | | | | |
| CH2 | 357.97 | 0.76 | 34.45 | 18.77 | 46.02 | 1.16 | 28.63 | 70.21 |
| CH5 | 247.77 | 1.85 | 24.56 | 22.65 | 50.94 | 2.45 | 30.02 | 67.52 |
| CH5 | 268.40 | | DOLERITE | | | | | |
| CH5 | 283.00 | 2.43 | 48.50 | 6.57 | 42.50 | 4.72 | 12.76 | 82.52 |
| CH5 | 294.30 | | DOLERITE | | | | | |
| CH5 | 325.77 | 2.21 | 31.35 | 23.61 | 42.83 | 3.22 | 34.39 | 62.39 |
| CH5 | 335.26 | 1.37 | 17.26 | 22.11 | 59.25 | 1.66 | 26.72 | 71.61 |
| CH5 | 344.10 | 2.27 | 57.05 | 8.38 | 32.30 | 5.29 | 19.51 | 75.20 |
| CH6 | 319.59 | 5.99 | 42.21 | 23.38 | 28.41 | 10.37 | 40.46 | 49.16 |
| CH6 | 328.84 | 5.27 | 16.07 | 34.62 | 44.04 | 6.28 | 41.25 | 52.47 |
| CH6 | 340.05 | 4.98 | 13.60 | 32.00 | 49.41 | 5.76 | 37.04 | 57.19 |
| CH6 | 355.50 | 2.42 | 63.10 | 13.18 | 21.30 | 6.56 | 35.72 | 57.72 |
| CH7 | 403.83 | 6.36 | 29.78 | 32.85 | 31.01 | 9.06 | 46.78 | 44.16 |
| CH7 | 462.86 | 3.72 | 12.91 | 32.05 | 51.33 | 4.27 | 36.80 | 58.94 |
| CH7 | 485.62 | 1.30 | 22.10 | 9.42 | 67.18 | 1.67 | 12.09 | 86.24 |
| CH9 | 405.70 | 3.81 | 39.94 | 22.04 | 34.21 | 6.34 | 36.70 | 56.96 |
| CH9 | 419.60 | | DOLERITE | | | | | |
| CH9 | 420.80 | 1.52 | 58.09 | 6.03 | 34.37 | 3.63 | 14.39 | 82.01 |
| CH9 | 444.21 | 1.91 | 40.61 | 15.51 | 41.97 | 3.22 | 26.12 | 70.67 |
| CH9 | 455.90 | | DOLERITE | | | | | |

M% (ad) moisture present percentage in dry basis, A(ad)% ash present in dry basis, VM(ad)% volatile matter present percentage in dry basis, FC(ad)% fixed carbon present percentage in dry ash-free basis, M%(daf) moisture present in dry ash-free basis, VM(daf)% volatile matter present percentage in dry ash-free basis, FC(daf)% fixed carbon present percentage in dry ash-free basis.

### 4.3. The Passey's TOC outputs

Passey's method has been extensively utilised to determine the organic richness of rock. Passey's TOCs and TOCd were determined using equations:

$$TOCs = SlogR * 10^{\wedge} (0.297 - 0.1688 * LOM) \quad (2)$$

$$TOCd = DlogR * 10^{\wedge} (0.297 - 0.1688 * LOM) \quad (3)$$

Borehole CH1 did not intercept any dolerite, all samples are immature, but high resistivity responses observed at depth 275.0 m–277.30 m indicate early biogenic gas generation. The correlation between Carbon at dry ash-free (daf %) and calculated TOC of boreholes CH1 and CH7 of the non-heat affected and heat affected boreholes (Fig. 8) showed that TOCs calculated from the sonic log displayed a better correlation than that of density log (TOCd). A coefficient of determination of $R^2 = 0.85$ (CH1) and 0.48 (CH7) was determined from TOCs, whereas the TOCd calculated from the sonic log showed a coefficient of determination of 0.47(CH1) and 0.25 (CH7), respectively.

The heat affected samples at depth 276.51 m and 357.97 m of borehole CH2 showed very high LOM (Table 3) and a high value of fixed carbon (Table 4). This can also be observed in heat-affected samples of all the other boreholes. The sample at depth 357.97 m has been metamorphosed to hard carbonaceous coal; this, coupled with a comparatively higher LOM, has immensely affected the TOC outputs.

Passey et al. (1990) stated that TOCs accuracy is superior to logs TOCd and suggested that this could be due to the sensitivity of density logs to adverse hole conditions and heavy minerals such as pyrite. In this study, TOCs do not display any superiority to TOCd; its accuracy is poorer than TOCd. The density of the samples controls both density and sonic log readings. Most sampled intervals are pyritic and do not necessarily exhibit higher densities due to their presence. Passey's method is helpful in identifying coal as organic-rich zones and potential source rocks. However, accuracy in its TOCs/TOCd predictions depends on selected baseline readings, density and more so, on the LOM of the coal. LOM has proved to be a significant and sensitive parameter in this method.

Coal that has undergone normal burial metamorphism compositionally varies from the rapidly heat altered coal. The $R_o$ increased from 0.44 in non-heat affected coal to 5.53 in the contact metamorphism zone (Table 3). Adjacent to the intrusion, there is a decrease in the volatile matter; moisture initially decreases then slightly increases as sealed by the intrusion; the fixed carbon initially increases then decreases as vitrinite decomposes and semi-coke begins to form. Ash yield increases adjacent to the intrusion. According to Rimmer et al. (2009), these geochemical changes reflect increasing rank approaching the intrusion.

### 4.4. Application of Passey's ΔLogR: generating TOC curves

The vitrinite reflectance measurement was conducted on 41 cored intervals. In the remaining intervals, LOM is estimated; however, this has been done in boreholes CH1 and CH6, where maturity is believed to have been due to the normal coalification process. LOM ranges are 7.72–8 and 7.86 to 8.68 for CH1 and CH6, respectively (Table 3). Therefore, in both boreholes, an average LOM value within a reasonable range can be used to generate TOC estimation curves for the entire borehole. In dolerite heat influenced boreholes, using an average LOM would lead to very erroneous TOC

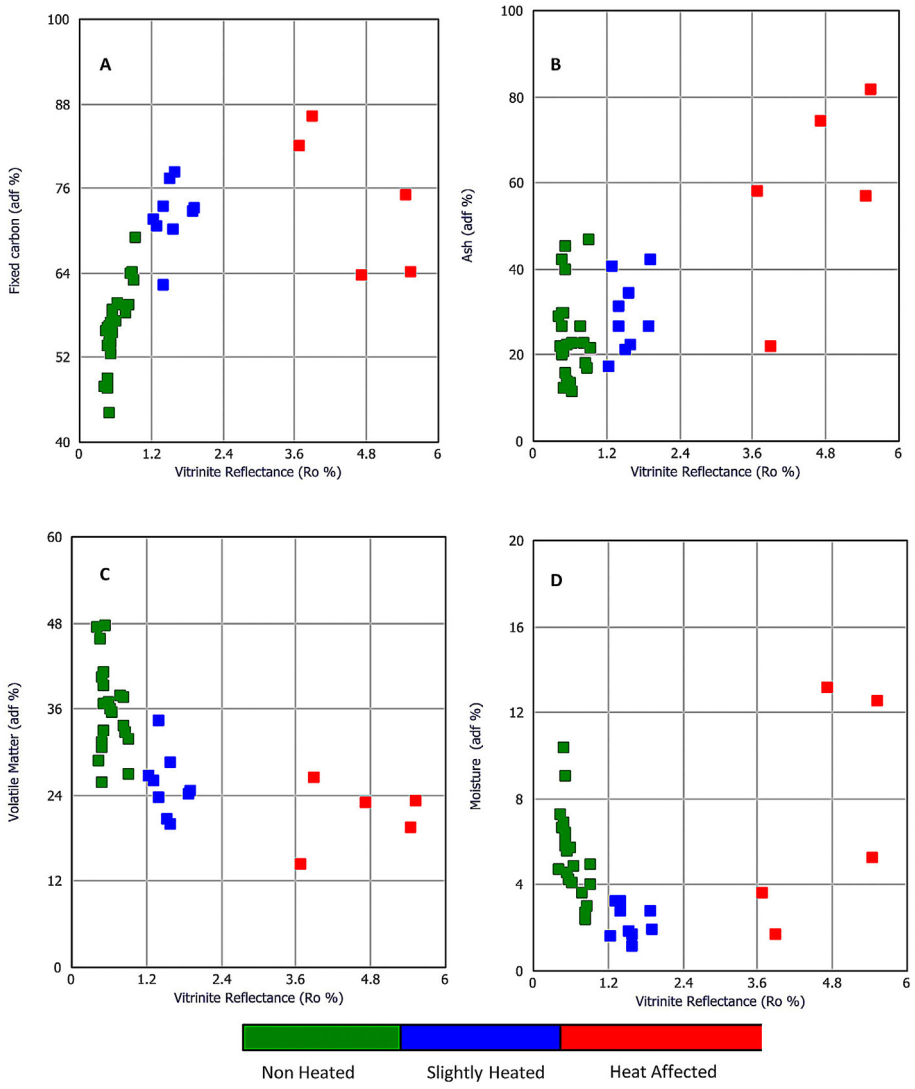


**Fig. 7.** Correlations between $R_o$ and proximate analysis results. (a) Fixed Carbon Vs $R_o$, (b) ash content Vs $R_o$, (c) volatile matter Vs $R_o$, and (d) Moisture content Vs $R_o$. Cluster 1(green colour) represents non-heat affected, cluster 2 (blue colour) represents slightly heat-affected, and Cluster 3 (red colour) represents devolatilized heat-affected samples.

estimates as the LOM ranges are too broad and are not depth dependant. For example, CH4 and CH7 display LOM ranges of 9.52–19.26 and 8 to 18.13, respectively.

Fig. 9 and Fig. 10 (track 7) indicate that TOCs estimations are more robust than TOCd in both boreholes. Essentially in both boreholes, Passey's TOC curves mostly align well with the carbon measurements. Although not accurate, the curves indicate that the method can be applied to coal that has not been thermally altered by igneous sills and dykes.

## 5. Conclusions and recommendations

Passey's method is successfully used to determine total organic carbon (TOC) from boreholes in Botswana's Kalahari Basin. Results of Passey's method compared with laboratory-measured carbon showed that Passey's method effectively identifies coal intervals. However, the method works poorly in coal metamorphosed by dolerite intrusions. The heat affected coal samples had $R_o$ from 0.77 to 5.53 and increased in maturity from primary maceral controlled to high volatile bituminous and anthracite coal. Proximate analysis showed compositional changes in the coal were controlled by proximity to sill intrusion, with a decrease in Fixed Carbon and an increase in ash yield in the contact metamorphism zone. The method works well for the unaltered coal that has undergone burial maturation displaying $R_o$ of 0.44–0.65. In unintruded boreholes, correlations between carbon and calculated TOC indicate strong relationships. This study has demonstrated that TOC calculated from the sonic log is more reliable in coal not affected by contact metamorphism than TOC calculated from the density log.

One of the significant shortcomings of Passey's method is selecting the subjective baseline interval. Also, heterogeneity of shale sequences could result in high uncertainties for calculated TOC. Although coals generally have high carbon contents, it is possible that minor carbonate quantities may have contributed to

**Table 5**
Ultimate analysis results.

| Borehole | Top Depth (m) | Carbon (% d.a.f) | Hydrogen (% d.a.f) | Nitrogen (% d.a.f) | Sulphur (% d.a.f) | Oxygen (% d.a.f) | H/C | O/C |
|---|---|---|---|---|---|---|---|---|
| CH1 | 245.82 | 76.1 | 5.05 | 1.53 | 1.9 | 15.4 | 0.07 | 0.20 |
| CH1 | 268.38 | 76.7 | 4.92 | 1.5 | 2.7 | 14.2 | 0.06 | 0.19 |
| CH1 | 275.24 | 77.8 | 4.71 | 1.57 | 1.56 | 14.4 | 0.06 | 0.19 |
| CH1 | 277.30 | 74.7 | 4.97 | 1.61 | 3.2 | 15.5 | 0.07 | 0.21 |
| CH1 | 279.96 | 76.6 | 5.12 | 1.69 | 2.69 | 13.9 | 0.07 | 0.18 |
| CH3 | 364.70 | 79.5 | 4.88 | 1.46 | 3.04 | 11.1 | 0.06 | 0.14 |
| CH3 | 374.94 | 71.8 | 5.52 | 1.58 | 1.66 | 19.4 | 0.08 | 0.27 |
| CH3 | 410.45 | 78.5 | 4.58 | 1.68 | 0.6 | 14.6 | 0.06 | 0.19 |
| CH3 | 417.95 | 83.4 | 3.74 | 2.17 | 2.59 | 8.1 | 0.04 | 0.10 |
| CH3 | 420.95 | 85.1 | 3.87 | 2.06 | 0.48 | 8.5 | 0.05 | 0.10 |
| CH5 | 247.77 | 80.3 | 4.94 | 1.14 | 6.62 | 6.7 | 0.06 | 0.08 |
| CH5 | 283.00 | 91 | 1.25 | 0.64 | 3.04 | 4.1 | 0.01 | 0.05 |
| CH5 | 325.77 | 78.8 | 4.63 | 1.78 | 1.03 | 13.8 | 0.06 | 0.18 |
| CH5 | 335.26 | 84.8 | 4.28 | 1.92 | 0.87 | 8.1 | 0.05 | 0.10 |
| CH5 | 344.10 | 85.7 | 2.84 | 1.16 | 0.24 | 10.1 | 0.03 | 0.12 |
| CH6 | 319.59 | 73.2 | 5.44 | 1.25 | 5.61 | 14.5 | 0.07 | 0.20 |
| CH6 | 328.84 | 78 | 5.31 | 1.49 | 1.97 | 13.2 | 0.07 | 0.17 |
| CH6 | 340.05 | 77.3 | 4.93 | 1.68 | 0.65 | 15.4 | 0.06 | 0.20 |
| CH6 | 355.50 | 71.1 | 5.51 | 1.38 | 0.35 | 21.7 | 0.08 | 0.31 |
| CH7 | 403.83 | 75.9 | 4.87 | 1.46 | 2.82 | 15 | 0.06 | 0.20 |
| CH7 | 432.36 | 78.4 | 5.14 | 1.54 | 1.15 | 13.8 | 0.07 | 0.18 |
| CH7 | 439.95 | 78.5 | 5.22 | 1.72 | 0.75 | 13.8 | 0.07 | 0.18 |
| CH7 | 462.86 | 79.1 | 5.04 | 1.95 | 0.85 | 13.1 | 0.06 | 0.17 |
| CH7 | 485.62 | 89.3 | 2.95 | 1.8 | 1.19 | 4.8 | 0.03 | 0.05 |
| CH8 | 370.48 | 75.3 | 5.39 | 1.51 | 10.55 | 7.3 | 0.07 | 0.10 |
| CH8 | 383.62 | 79.6 | 5.12 | 1.6 | 2.95 | 10.7 | 0.06 | 0.13 |
| CH8 | 387.88 | 80.7 | 5.17 | 1.16 | 2.43 | 10.1 | 0.06 | 0.13 |
| CH9 | 405.70 | 74.7 | 5.26 | 1.48 | 5.27 | 13.3 | 0.07 | 0.18 |
| CH9 | 420.80 | 87.8 | 3.48 | 1.92 | 0.55 | 6.3 | 0.04 | 0.07 |
| CH9 | 444.21 | 83.9 | 4.62 | 1.92 | 2.2 | 7.4 | 0.06 | 0.09 |
| CH9 | 504.60 | 76.7 | 4.23 | 1.34 | 0.61 | 17.1 | 0.06 | 0.22 |
| CH9 | 520.86 | 83.5 | 4.38 | 1.99 | 4.03 | 6.1 | 0.05 | 0.07 |

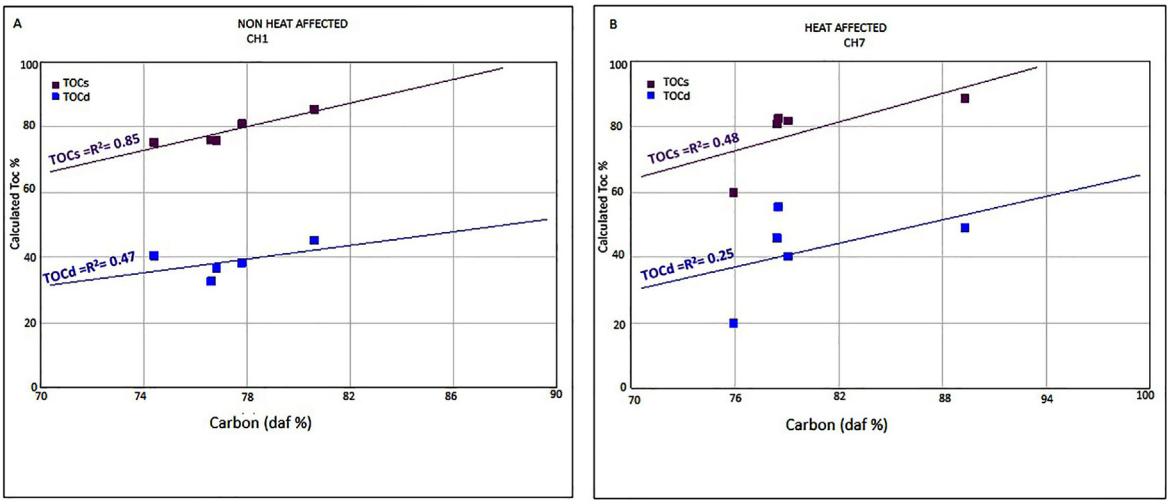


**Fig. 8.** Plot of calculated TOC against the fixed carbon (daf.%) for non-heat-affected and heat-affected boreholes. (a) Non-heat-affected borehole (CH1) presenting an excellent relationship between calculated TOCd and fixed carbon and fair TOCs. (b)The heat affected (CH7) presenting a fair and poor relationship between TOC and fixed carbon.

the total carbon amount and may be the cause of inaccuracy in some calculated TOC using the ΔLogR technique as it only detects organic carbon. Thus, it is recommended that Rock-Eval pyrolysis be conducted on decarbonated coal samples to provide direct TOC measurements.

## Declaration of competing interest

The authors declare that they have no known competing financial interests or personal relationships that could have appeared to influence the work reported in this paper.

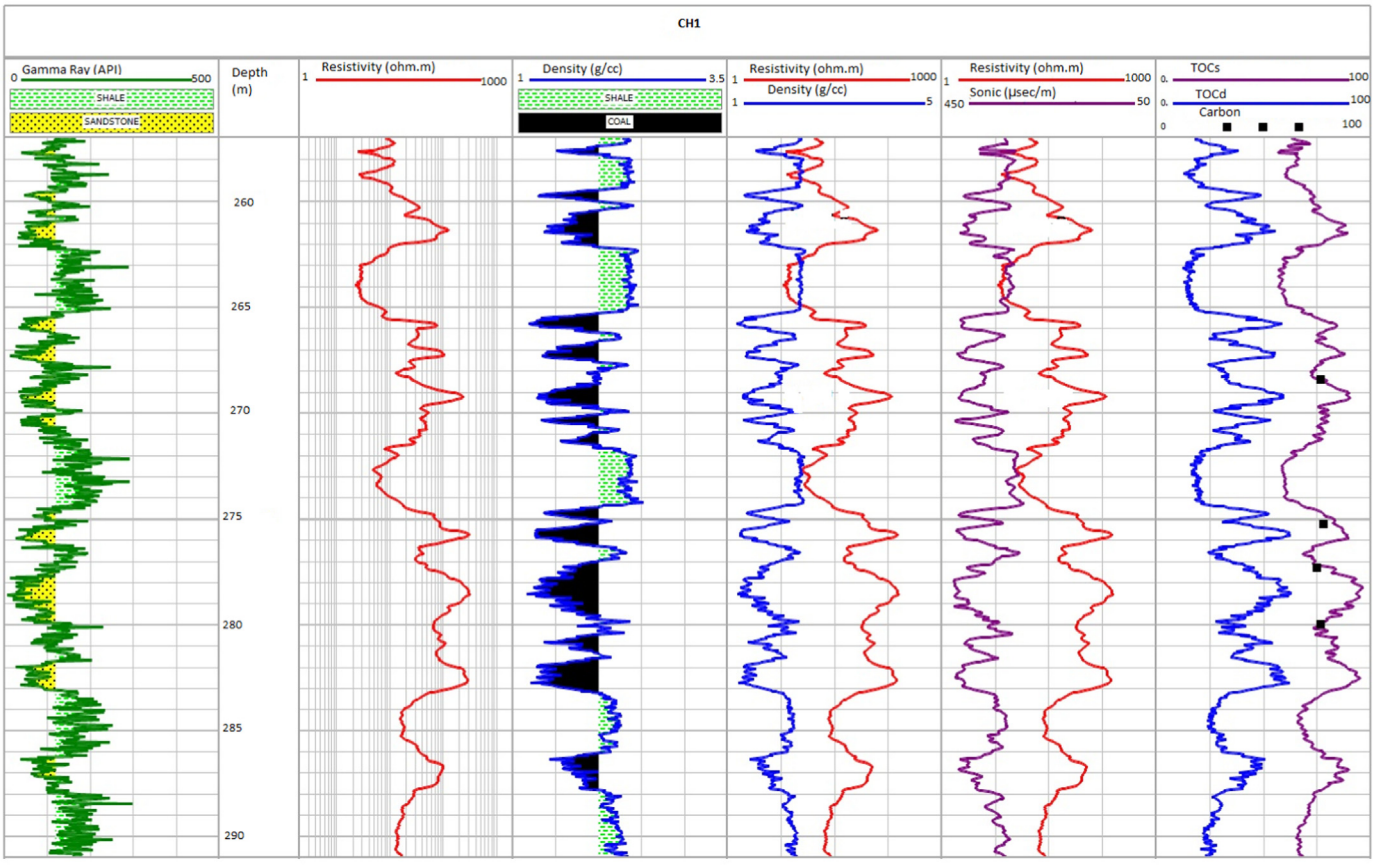


**Fig. 9.** Present log evaluation results for TOC for borehole CH1(non-heat affected). The 1st track is GR, and the 2nd track is the depth curve. The 3rd track shows the resistivity, and the 4th track shows the density curve. The 5th track is the overlay of resistivity with density, and the 6th track is the overlay of resistivity with the sonic curve. The 7th track shows a comparison of TOCds, TOCs curves and fixed carbon (black dots). Good agreement between TOCd and fixed carbon was observed, indicating the effectiveness and reliability of the TOCd in non-heat affected coal.

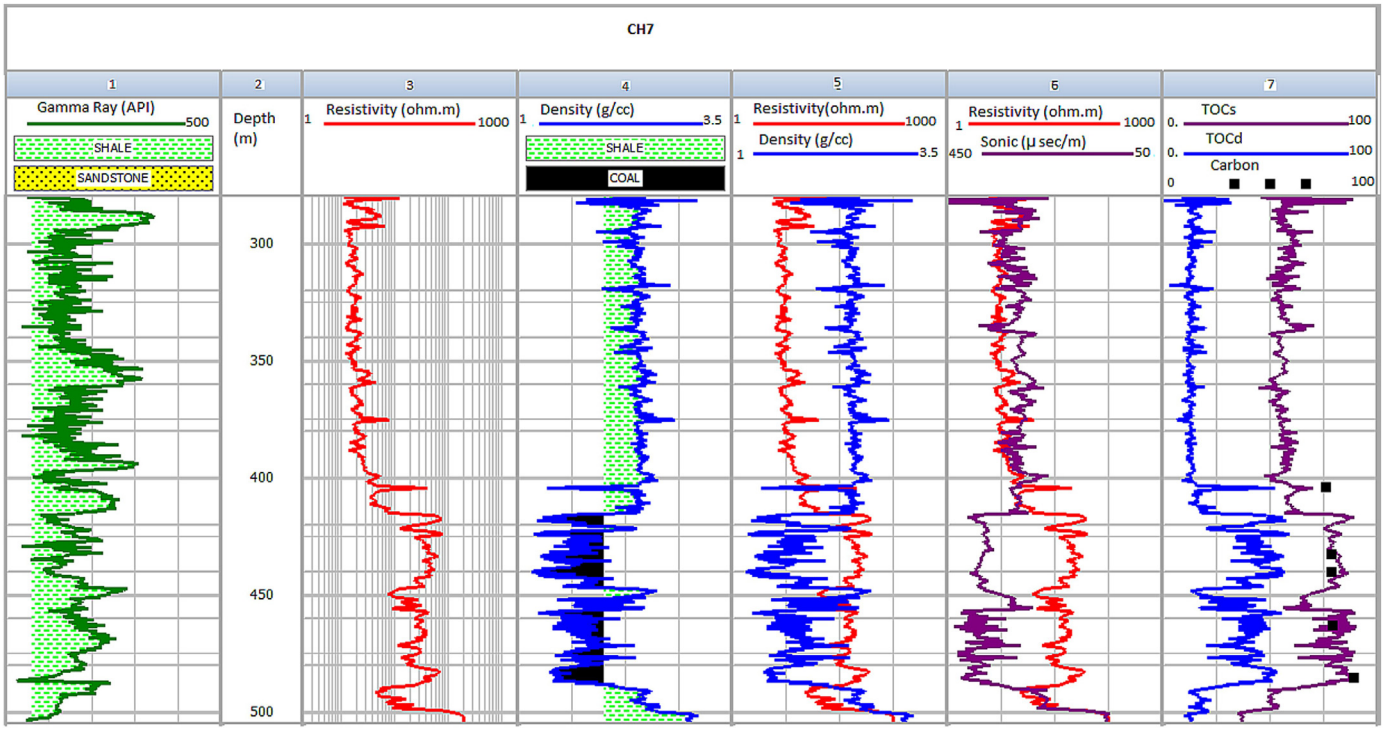


**Fig. 10.** Presentation of log evaluation results for TOC for borehole CH7(heat affected). The 1st track is GR, and the 2nd track is the depth curve. The 3rd track shows the resistivity, and the 4th track shows the density curve. The 5th track is the overlay of resistivity with density, and the 6th track is the overlay of resistivity with the sonic curve. The 7th track shows a comparison of TOCds, TOCs curves and fixed carbon (black dots). The data show poor agreement between TOCd and fixed carbon, thereby indicating the unreliability of the TOCd in heat-affected coal.

## Acknowledgement

The authors would like to thank Sasol Exploration and Production International (SEPI) for providing the data used in this work. Sincere thanks to Mr Christopher Mclean, Mr Junior Potgieter, Mr Ben Egbe, and Mr Hanno van Staden for their guidance and contribution. Senergy Company is also acknowledged for providing the IP software package.

## References

Akanksha, Singh, A.K., Mohanty, D., Jena, H.M., Panwar, D.S., 2020. Prospective evaluation of hydrocarbon generation potential of Umarsar lignite, India. Energy Sources, Part A Recovery, Util. Environ. Eff. 42, 664–675.
Alfred, D., Vernik, L., 2012. A New Petrophysical Model for Organic Shales, 53rd Annual Logging Symposium. SPWLA.
Amini, M., MirMostafaee, S., Ahmadi, J., 2014. Log-gamma-generated families of distributions. Statistics 48, 913–932.
Amiri Bakhtiar, H., Telmadarreie, A., Shayesteh, M., Heidari Fard, M.H., Talebi, H., Shirband, Z., 2011. Estimating total organic carbon content and source rock evaluation, applying ΔlogR and neural network methods: Ahwaz and Marun oilfields, SW of Iran. Petrol. Sci. Technol. 29, 1691–1704.
Asquith, G.B., Gibson, C.R., 1982. Basic Relationships of Well Log Interpretation: Chapter I. AAPG Special Volumes, pp. 1–27.
Ayodele, O.L., Chatterjee, T.K., Opuwari, M., 2021. Static reservoir modeling using stochastic method: a case study of the cretaceous sequence of Gamtoos Basin, Offshore, South Africa. J. Pet. Explor. Prod. Technol. 11, 4185–4200.
Banik, P., 2020. Laboratory investigation of coal characteristics from Tikak Parbat formation of Nort-East India for coal bed methane study. J. Pet. Explor. Prod. Technol. 10, 2631–2636.
Bennett, J.D., 1989. Review of Lower Karoo coal basins and coal resource development in parts of central and southern Africa with particular reference to northern Malawi. Br. Geol. Surv. 89 (21), 1–73.
Bordy, E.M., Segwabe, T., Makuke, B., 2010a. Sedimentology of the upper triassic–lower Jurassic (?) mosolotsane formation (Karoo supergroup), Kalahari Karoo basin, Botswana. J. Afr. Earth Sci. 58, 127–140.
Bordy, E.M., Segwabe, T., Makuke, B., 2010b. Sedimentology of the upper triassic–lower Jurassic (?) mosolotsane formation (Karoo supergroup), Kalahari Karoo basin, Botswana. J. Afr. Earth Sci. 58, 127–140.
Bostick, N.H., Pawlewicz, M.J., 1984. Paleotemperatures based on vitrinite reflectance of shales and limestone in igneous dike aureoles in the Upper Cretaceous Pierre shale, Walsenburg, Colorado. In: Woodward, J.G., Meissner, F.F., Clayton, C.J. (Eds.), Hydrocarbon Source Rocks of the Greater Rocky Mountain Region. Rocky Mountain Association of Geologists, pp. 387–392.
Bulguroglu, M.E., Milkov, A.V., 2020. Thickness matters: influence of dolerite sills on the thermal maturity of surrounding rocks in a coal bed methane play in Botswana. Mar. Petrol. Geol. 111, 219–229.
Catuneanu, O., Wopfner, H., Eriksson, P.G., Cairncross, B., Rubidge, B.S., Smith, R.M.H., Hancox, P.J., 2005. The Karoo basins of south-central Africa. J. Afr. Earth Sci. 43, 211–253.
Charsky, A., Herron, S., 2013. Accurate, Direct Total Organic Carbon (TOC) Log from a New Advanced Geochemical Spectroscopy Tool: Comparison with Conventional Approaches for TOC Estimation. AAPG Annual Convention and Exhibition, Pittsburg, pp. 19–22.
Cokar, M., Kallos, M., Huang, H., Larter, S., Gates, I.D., 2010. Biogenic Gas Generation from Shallow Organic-Matter-Rich Shales. Canadian Unconventional Resources and International Petroleum Conference, Society of Petroleum Engineers.
Diesel, C.F.K., 1992. Coal-bearing Depositional Systems. Springer, Berlin, p. 721.
Elder, J.P., 1983. Proximate analysis by automated thermogravimetry. Fuel 62, 580–584.
Faiz, M., Crozier, E., Lee-King, A., 2013. Influence of Coal Type, Rank and Thermal History on Gas Contents in the Kubu PLs, Botswana. Kubu Energy, Brisbane.
Fertl, W.H., Chilingar, G.V., 1988. Total organic carbon content determined from well logs. SPE Form. Eval. 3, 407–419.
Fjeldskaar, W., Helset, H.M., Johansen, H., Grunnaleite, I., Horstad, I., 2008. Thermal modelling of magmatic intrusions in the Gjallar Ridge, Norwegian Sea: implications for vitrinite reflectance and hydrocarbon maturation. Basin Res. 20, 143–159.
Franchi, F., Kelepile, T., Di Capua, A., De Wit, M.C., Kemiso, O., Lasarwe, R., Catuneanu, O., 2021. Lithostratigraphy, sedimentary petrography and geochemistry of the upper Karoo supergroup in the central Kalahari Karoo subbasin, Botswana. J. Afr. Earth Sci. 173, 104025.
Golab, A., 2003. The Impact of Igneous Intrusions on Coal, Cleat Carbonate, and Groundwater Composition. University of Wollongong.
Haddon, I.G., 2005. The Sub-kalahari Geology and Tectonic Evolution of the Kalahari Basin, Southern Africa. University of the Witwatersrand, Johannesburg.
Hood, A., Gutjahr, C.C.M., Heacock, R.L., 1975. Organic metamorphism and the generation of petroleum. AAPG (Am. Assoc. Pet. Geol.) Bull. 59, 986–996.
Jarvie, D.M., 2012. Shale resource systems for oil and gas: Part 2—shale-oil resource systems. AAPG Memoir 97. https://doi.org/10.1306/13321446M973489.
Jiang, J.-Y., Cheng, Y.-P., Wang, L., Li, W., Wang, L., 2011. Petrographic and geochemical effects of sill intrusions on coal and their implications for gas outbursts in the Wolonghu Mine, Huaibei Coalfield, China. Int. J. Coal Geol. 88, 55–66.
Johnson, M.R., Van Vuuren, C.J., Hegenberger, W.F., Key, R., Show, U., 1996. Stratigraphy of the Karoo supergroup in southern Africa: an overview. J. Afr. Earth Sci. 23, 3–15.
Kalkreuth, W., Levandowski, J., Weniger, P., Krooss, B., Prissang, R., da Rosa, A.L., 2020. Coal characterization and coalbed methane potential of the Chico-Lomã Coalfield, Paraná Basin, Brazil—Results from exploration borehole CBM001-CL-RS. Energy Explor. Exploit. 38, 1589–1630.
Kamali, M.R., Mirshady, A.A., 2004. Total organic carbon content determined from well logs using ΔLogR and Neuro Fuzzy techniques. J. Petrol. Sci. Eng. 45, 141–148.
Langenberg, W., Macdonald, D., Kalkreuth, W., 1992. Sedimentologic and tectonic controls on coal quality of a thick coastal plain coal in the foothill of Alberta, Canada. Geol. Soc. Am. 267, 101–116.
Le Gall, B., Tshoso, G., Jourdan, F., Féraud, G., Bertrand, H., Tiercelin, J.-J., Kampunzu, A.B., Modisi, M.P., Dyment, J., Maia, M., 2002. 40Ar/39Ar geochronology and structural data from the giant Okavango and related mafic dyke swarms, Karoo igneous province, northern Botswana. Earth Planet Sci. Lett. 202, 595–606.
Li, G., Yan, D., Zhuang, X., Zhang, Z., Fu, H., 2019. Implications of the pore pressure and in situ stress for the coalbed methane exploration in the southern Junggar Basin, China. Eng. Geol. 262, 105305.
Li, J., Lu, J., Li, Z., Wu, Q.Z., Nan, Z., 2014. Four-pore'modeling and its quantitative logging description of shale gas reservoir. Oil Gas Geol. 35, 266–271.
Liu, C., Zhao, W., Sun, L., Zhang, Y., Chen, X., Li, J., 2021. An improved ΔlogR model for evaluating organic matter abundance. J. Petrol. Sci. Eng. 206, 109016.
Mabitje, M.S., 2016. Determination of Total Organic Carbon Content Using Passey's ΔLogR Method in Coals of the Central Kalahari Karoo Basin, Botswana. Master of Science thesis. University of the Western Cape, Republic of South Africa.
Magoba, M., Opuwari, M., 2020. Petrophysical interpretation and fluid substitution modelling of the upper shallow marine sandstone reservoirs in the Bredasdorp Basin, offshore South Africa. J. Pet. Explor. Prod. Technol. 10, 783–803.
Mayoral, M.C., Izquierdo, M.T., Andrés, J.M., Rubio, B., 2001. Different approaches to proximate analysis by thermogravimetry analysis. Thermochim. Acta 370, 91–97.
Mendhe, V.A., 2020. Coal seam reservoir characteristics for coalbed methane in North and South Karanpura coalfields, Jharkhand. Gondwana Geol. Mag. 12, 141–152.
Modie, B.N., Le Hérissé, A., 2009. Late palaeozoic palynomorph assemblages from the Karoo supergroup and their potential for biostratigraphic correlation, Kalahari Karoo basin, Botswana. Bull. Geosci. 84, 337–358.
Mohammed, S., Opuwari, M., Titinchi, S., 2020. Source rock evaluation of Afowo clay type from the Eastern Dahomey Basin, Nigeria: insights from different measurements. Sci. Rep. 10, 1–13.
Mohammed, S., Opuwari, M., Titinchi, S., Bata, T., Abubakar, M.B., 2019. Evaluation of source rock potential and hydrocarbon composition of oil sand and associated clay deposits from the Eastern Dahomey Basin, Nigeria. J. Afr. Earth Sci. 160, 103603.
Moore, T.A., 2012. Coalbed methane: a review. Int. J. Coal Geol. 101, 36–81.
Nyakilla, E.E., Silingi, S.N., Shen, C., Jun, G., Mulashani, A.K., Chibura, P.E., 2022. Evaluation of source rock potentiality and prediction of total organic carbon using well log data and integrated methods of multivariate analysis, machine learning, and geochemical analysis. Nat. Resour. Res. 31, 619–641.
Ogala, J.E., 2011. Hydrocarbon potential of the upper cretaceous coal and shale units in the Anambra basin, southeastern Nigeria. Petrol. Coal 53, 35–44.
O'Keefe, J.M., Bechtel, A., Christanis, K., Dai, S., DiMichele, W.A., Eble, C.F., Esterle, J.S., Mastalerz, M., Raymond, A.L., Valentim, B.V., 2013. On the fundamental difference between coal rank and coal type. Int. J. Coal Geol. 118, 58–87.
Opuwari, M., 2010. Petrophysical Evaluation of the Albian Age Gas Bearing Sandstone Reservoirs of the OM Field, Orange Basin, South Africa (PhD Thesis). University of the Western Cape.
Opuwari, M., Afolayan, B., Mohammed, S., Amaechi, P.O., Bareja, Y., Chatterjee, T., 2022. Petrophysical core-based zonation of OW oilfield in the Bredasdorp Basin South Africa. Sci. Rep. 12, 1–19.
Opuwari, M., Bialik, O.M., Taha, N., Waldmann, N.D., 2021. The role of detrital components in the petrophysical parameters of Paleogene calcareous-dominated hemipelagic deposits. Arabian J. Geosci. 14, 1–13.
Opuwari, M., Dominick, N., 2021. Sandstone reservoir zonation of the northwestern Bredasdorp Basin South Africa using core data. J. Appl. Geophys. 193, 104425.
Panwar, D.S., Suman, S., Singh, A.K., Saxena, V.K., Chaurasia, R.C., 2020. Assessment of hydrocarbon generation potential of bituminous coal from Raniganj Basin, India. Energy Sources, Part A Recovery, Util. Environ. Eff. 42, 824–834.
Passey, Q.R., Creaney, S., Kulla, J.B., Moretti, F.J., Stroud, J.D., 1990. A practical model for organic richness from porosity and resistivity logs. AAPG (Am. Assoc. Pet. Geol.) Bull. 74, 1777–1794.
Price, L.C., 1983. Geologic time as a parameter in organic metamorphism and vitrinite reflectance as an absolute paleogeothermometer. J. Petrol. Geol. 6 (1), 5–37.
Ramiah, K., Trivedi, K.B., Opuwari, M., 2019. A 2D geomechanical model of an offshore gas field in the Bredasdorp Basin, South Africa. J. Pet. Explor. Prod. Technol. 9, 207–222.
Rao, P.L.S., Rasheed, M.A., Hasan, S.Z., Rao, P.H., Harinarayana, T., 2014. Role of

geochemistry in coalbed methane-A review. Geosciences 4, 29–32.
Rider, M, 2002. The Geological Interpretation of Well Logs. Rider-French Consulting Ltd, Sutherland.
Rider, M., Kennedy, M., 2002. The Geological Interpretation of Well Logs. Rider-French Consulting Ltd, Sutherland.
Rimmer, S.M., Yoksoulian, L.E., Hower, J.C., 2009. Anatomy of an intruded coal, I: effect of contact metamorphism on whole-coal geochemistry, Springfield (No. 5) (Pennsylvanian) coal, Illinois Basin. Int. J. Coal Geol. 79, 74–82.
Saffou, E., Raza, A., Gholami, R., Croukamp, L., Elingou, W.R., van Bever Donker, J., Opuwari, M., Manzi, M.S., Durrheim, R.J., 2020. Geomechanical characterization of $CO_2$ storage sites: a case study from a nearly depleted gas field in the Bredasdorp Basin, South Africa. J. Nat. Gas Sci. Eng. 81, 103446.
Sahoo, T.R., Funnell, R.H., Brennan, S.W., Sykes, R., Thrasher, G.P., Adam, L., Lawrence, M.J.F., Kellett, R.L., Ma, X., 2021. Delineation of coaly source rock distribution and prediction of organic richness from integrated analysis of seismic and well data. Mar. Petrol. Geol. 125.
Shiri, M., Ranjbar-Karami, R., Moussavi Harami, S.R., Rezaee, M., 2013. Evaluation of organic carbon content and source rock maturity using petrophysical logs and geochemical data: case study of Horn Valley Siltstone source rock, Amadeus Basin, Central Australia. J. Zankoy Sulaimani A 15, 145–158.
Singh, M.P., Singh, P.K., 1994. Indications of hydrocarbon generation in the coal deposits of the Rajmahal Basin, Bihar-revelations of fluorescence microscopy. J. Geol. Soc. India 43, 647–658.
Singh, P.K., 2012. Petrological and geochemical considerations to predict oil potential of Rajpardi and Vastan lignite deposits of Gujarat, Western India. J. Geol. Soc. India 80, 759–770.
Singh, P.K., 2011. Geological and petrological considerations for coal bed methane exploration: a review. Energy Sources, Part A Recovery, Util. Environ. Eff. 33, 1211–1220.
Singh, P.K., Singh, V.K., Rajak, P.K., Singh, M.P., Naik, A.S., Raju, S.V., Mohanty, D., 2016. Eocene lignites from Cambay basin, Western India: an excellent source of hydrocarbon. Geosci. Front. 7, 811–819.
Singh, V.K., Rajak, P.K., Singh, P.K., 2019. Revisiting the paleomires of western India: an insight into the early Paleogene lignite Corridor. J. Asian Earth Sci. 171, 363–375.
Smith, R.A., 1984. The lithostratigraphy of the Karoo Supergroup in Botswana. A report on the geophysical and geological results of follow-up drilling to the Aeromagnetic Survey of Botswana. Bull. Geol. Surv. Botswana 26, 1- 239.
Sondergeld, C.H., Newsham, K.E., Comisky, J.T., Rice, M.C., Rai, C.S., 2010. Petrophysical Considerations in Evaluating and Producing Shale Gas Resources. SPE Unconventional Gas Conference. Society of Petroleum Engineers.
Song, Y., Ma, X., Liu, S., Jiang, L., Hong, F., Qin, Y., 2018. Accumulation conditions and key technologies for exploration and development of Qinshui coalbed methane field. Petrol. Res. 3, 320–335.
Standards Association of Australia, 2000a. Australian Standards AS1038.3: Proximate Analysis of Higher Rank Coal. Standards Association of Australia, Sydney.
Standards Association of Australia, 2000b. Australian Standards AS2456.3: Microscopical Determination of the Reflectance of Coal Macerals. Standards Association of Australia, Sydney.
Stewart, A.K., Massey, M., Padgett, P.L., Rimmer, S.M., Hower, J.C., 2005. Influence of a basic intrusion on the vitrinite reflectance and chemistry of the Springfield (No. 5) coal, Harrisburg, Illinois. Int. J. Coal Geol. 63, 58–67.
Sun, S.Z., Sun, Y., Sun, C., Liu, Z., Dong, N., 2013. Methods of calculating total organic carbon from well logs and its application on rock's properties analysis. Geo Conv.: Integration 1–7.
Takahashi, K.U., Nakajima, T., Suzuki, Y., Morita, S., Sawaki, T., Hanamura, Y., 2020. Hydrocarbon generation potential and thermal maturity of coal and coaly mudstones from the Eocene Urahoro Group in the Kushiro Coalfield, eastern Hokkaido, Japan. Int. J. Coal Geol. 217, 103322.
Tao, S., Chen, S., Pan, Z., 2019. Current status, challenges, and policy suggestions for coalbed methane industry development in China: a review. Energy Sci. Eng. 7, 1059–1074.
Teichmüller, M., 1989. The genesis of coal from the viewpoint of coal petrology. Int. J. Coal Geol. 12, 1–87.
Trent, VA, Medlin, JH, Lynn, Coleman S, Stanton, RW, 1982. Chemical analyses and physical properties of 12 coal samples from the Pochontas field, Tazewell County, Virginia, and McDowell County, West Virginia. Geological Survey Bulletin, 1528.
Visser, J.N., 1997. Deglaciation sequences in the Permo-Carboniferous Karoo and Kalahari basins of southern Africa: a tool in the analysis of cyclic glaciomarine basin fills. Sedimentology 44, 507–521.
Wang, P., Chen, Z., Pang, X., Hu, K., Sun, M., Chen, X., 2016. Revised models for determining TOC in shale play: example from Devonian Duvernay shale, Western Canada sedimentary basin. Mar. Petrol. Geol. 70, 304–319.
Ward, C.R., Li, Z.S., Gurba, L.W., 2005. Variations in coal maceral chemistry with rank advance in the German Creek and Moranbah Coal Measures of the Brown Basin, Australia, using electron microprobe techniques. Int. J. Coal Geol. 63, 117–129.
Warne, S.S.J., 1991. Proximate analysis of coal, oil shale, low quality fossil fuels and related materials by thermogravimetry. TrAC, Trends Anal. Chem. 10, 195–199.
Yelwa, N.A., Mustapha, K.A., Opuwari, M., Aziz, A.A., 2021. Biomarkers, stable carbon isotope, and trace element distribution of source rocks in the Orange Basin, South Africa: implications for paleoenvironmental reconstruction, provenance, and tectonic setting. J. Pet. Explor. Prod. Technol. 12, 307–339.
Yi, L., Feng, J., Qin, Y., Li, W., 2017. Prediction of elemental composition of coal using proximate analysis. Fuel 197, 315–321.
Yu, H., Rezaee, R., Wang, Z., Han, T., Zhang, Y., Arif, M., Johnson, L., 2017. A new method for TOC estimation in tight shale gas reservoirs. Int. J. Coal Geol. 179, 269–277.
Zhang, S., Tang, S., Zhang, J., Pan, Z., 2018. Pore structure characteristics of China-sapropeliccoal and their development influence factors. J. Nat. Gas Sci. Eng. 53, 370–384.
Zhao, P., Ma, H., Rasouli, V., Liu, W., Cai, J., Huang, Z., 2017. An improved model for estimating the TOC in shale formations. Mar. Petrol. Geol. 83, 174–183.
Zhu, L., Zhang, C., Zhang, Z., Zhou, X., Liu, W., 2019. An improved method for evaluating the TOC content of a shale formation using the dual-difference ΔlogR method. Mar. Petrol. Geol. 102, 800–816.